Production of Na_2^+ by crossed-beam collisions in the presence of intense, nonresonant radiation

Jacques Boulmer* and John Weiner
Department of Chemistry, University of Maryland, College Park, Maryland 20742
(Received 15 October 1982)

We report the results of a battery of experiments to determine the origin of Na_2^+ produced by crossed sodium beams in the presence of intense optical radiation. The principal mechanism appears to be atomic collision combined with photon absorption. The characteristics of long-range optical collisions are compared with those expected from collisional resonances.

I. INTRODUCTION

Two recent papers[1,2] reporting the observation of Na^+ and Na_2^+ when sodium vapor is subjected to intense nonresonant optical radiation have excited much speculation concerning the origin of this effect. A common feature of these results is a highly structured spectrum covering a range from about 6000 to 5780 Å. Although the two most probable mechanisms to explain the presence of dimer ion appear to be laser-induced associative ionization[3−6] and three-photon photoionization of neutral dimer,[7−10] they are certainly not the only two candidates in the field. Significant improvements[9,11] in experimental design and laboratory instrumentation as well as marked advances in the spectroscopy of excited-state Na_2 now permit a deeper, more critical examination of the principal ionization mechanism.

The present paper reports a battery of experiments designed to distinguish among the several most plausible ionization pathways. From the results we conclude that the principal mechanism appears to be an atomic collision combined with photon absorption.

We begin by grouping the possible mechanisms into three main categories: (1) photoionization of Na_2; (2) excitation to real atomic or molecular excited states followed by collisional ionization; (3) laser-induced atomic collisions.
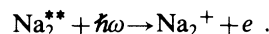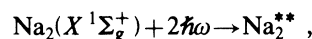
Photoionization itself can proceed by three different routes.

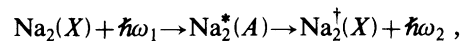(a) Two-step photon absorption followed by photoionization,

$$Na_2(X\,^1\Sigma_g^+)+\hbar\omega\rightarrow Na_2^*(A\,^1\Sigma_u^+)+\hbar\omega\rightarrow Na_2^{**} ,$$

$$Na_2^{**}+\hbar\omega\rightarrow Na_2^++e .$$
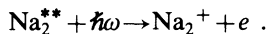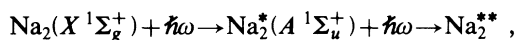
(b) Simultaneous two-photon absorption followed by photoionization,

$$Na_2(X\,^1\Sigma_g^+)+2\hbar\omega\rightarrow Na_2^{**} ,$$

$$Na_2^{**}+\hbar\omega\rightarrow Na_2^++e .$$

(c) Optical pumping of highly vibrationally excited $Na_2(X\,^1\Sigma_g^+)$ followed by either (a) or (b),

$$Na_2(X)+\hbar\omega_1\rightarrow Na_2^*(A)\rightarrow Na_2^\dagger(X)+\hbar\omega_2 ,$$

$$Na_2^\dagger(X)+2\hbar\omega\rightarrow Na_2^++e .$$

Category 2 processes, such as photoexcitation followed by *collisional* ionization in two discrete, noncoherent steps are easily imagined. For example, (a) population of $Na(3p)$ by an optical collision[12] followed by associative ionization,

$$Na(3s)+Na(3s)+\hbar\omega\rightarrow Na^*(3p)+Na(3s) ,$$

$$Na^*(3p)+Na^*(3p)\rightarrow Na_2^++e ,$$
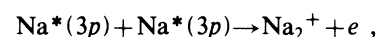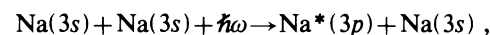
(b) photoexcitation of monomers or dimers followed by electron-impact ionization from energetic electrons heated by superelastic collisions,

$$Na_2+2\hbar\omega\rightarrow Na_2^{**} ,$$

$$Na_2^{**}+e\rightarrow Na_2^++e .$$
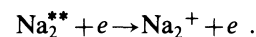
Ionization by superelastic collisions has been previously advanced to explain ionization by *resonant* radiation.[13]

The third category includes all processes in which photons are absorbed *simultaneously* with the collisional encounter. For example, (a) an optical collision followed immediately by two-photon ionization,

$$Na(3s)+Na(3s)+\hbar\omega\rightarrow[Na^*(3p)+Na(3s)]$$

$$+2\hbar\omega\rightarrow Na_2^++e ,$$
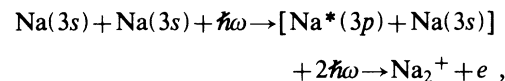
(b) an optical collision followed by resonance associ-
ation to a long-lived Na_2 quasimolecule followed by
two-photon ionization,

$$Na(3s) + Na(3s) + \hbar\omega \rightarrow [Na^*(3p) + Na(3s)]$$

(optical collision) ,

$$[Na^*(3p) + Na(3s)] \rightarrow [Na_2^*]$$
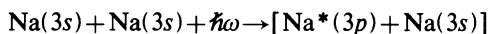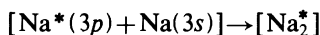
(collision resonance association) ,

$$[Na_2^*] + 2\hbar\omega \rightarrow Na_2{}^+$$

(quasimolecule photoionization). These two path-
ways (a) and (b) are illustrated in Fig. 7 and the dis-
tinction between them will be made clear in Sec. IV.

II. APPARATUS DESCRIPTION

Because we have modified substantially our exper-
imental setup since the last published reports,[12,14] we
describe here the present configuration. As before,
the heart of the apparatus is a stainless-steel cylin-
drical vessel, 33 cm long by 28 cm in diameter. A
ring of eight ports symmetrically placed around the
circumference defines the interaction plane perpen-
dicular to the cylinder axis. The entire assembly
mounts on a heavily reinforced aluminum table with
the interaction plane parallel and 13 cm above the
table surface. The vessel is evacuated by a conven-
tional diffusion pumping stack from which it can be
isolated by an electropneumatically controlled gate
valve. Two effusive atomic beam sources bolt
through the port ring at right angles to each other
and at 45° with respect to the axis of the laser beams
which pass between them (see Fig. 1). Each atomic
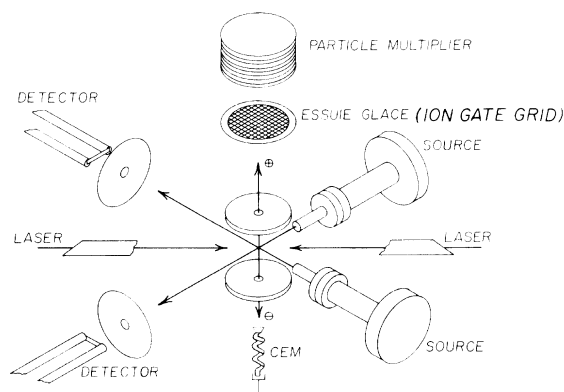beam source features a special flexible reentry

FIG. 1. Schematic diagram of the apparatus. Interac-
tion region is completely surrounded by liquid-nitrogen-
cooled baffles. The essuie-glace is a gated suppressor grid
to block distortion of weak $Na_2{}^+$ signals from strong Na^+
intensity.

mount on a standard vacuum flange to permit con-
venient angular and linear alignment. The sources
themselves are a double-oven design in which the
temperature of the primary oven defines the metal
vapor pressure and the secondary or nozzle oven su-
perheats the vapor to prevent clogging of the output
orifice and to suppress dimer concentration. The
secondary oven may be heated independently to
about 1100 °C for short times and 900 °C continuous-
ly. Thermocouple measurements confirm that heat
transfer between the two oven stages is slow and
inefficient. Hot-wire detectors monitor alkali-metal
beam intensity for a quick, approximate check, but
laser photoionization now provides a direct quanti-
tative measure of atomic and dimer density at the
collisional interaction region.[15]

As indicated in Fig. 1, ions produced synchro-
nously with the laser pulse are accelerated vertically
up a 15-cm time-of-flight drift tube and detected by
a particle multiplier. The acceleration field is pulsed
on about 20 nsec after the arrival of the laser pulse
and remains on for a 2-μsec duration. The ampli-
tude of the electric field is never more than 24
V/cm. A suppressor grid labeled ("essuie glace" in
Fig. 1) placed immediately before the particle multi-
plier selectively attenuates very large early arriving
ion bunches so as to measure higher mass but lower
intensity peaks without distortion. This feature is
especially useful for measuring weak $Na_2{}^+$ signals
in the presence of strong Na^+ intensity. Signal out-
put from the particle multiplier is buffered, ampli-
fied, and fed to a gated boxcar integrator. The gate
on the boxcar may be set to separately measure indi-
vidual mass peaks.

The schematic of Fig. 1 further shows provision
for monitoring electron production from the ioniza-
tion event with a channel electron multiplier (CEM)
situated below the collision plane. Speed of the
CEM response allows measurement of the time evo-
lution of the ionizing process to a precision of about
20 nsec. This time resolution is sufficient to permit
distinction between ionization processes which turn
on and turn off promptly with the laser pulse from
those with longer relaxation times.

For the sake of clarity we have not shown in Fig.
1 the photon-counting optical system which in other
experiments[15] monitors light emission from about
2200 to 9000 Å. Thus in principle (and in practice)
ion, electron, and photon production may be simul-
taneously detected in one experiment.

The single most important improvement, howev-
er, has been the inclusion of a commercial (Quantel)
Nd^{3+}:YAG pumped dye laser as the light source.
With this instrument we routinely produce un-
focused pulse power density of 10 MW/cm^2. Short
pulse duration (10 nsec) and good spectral resolution

$(<0.1$ cm$^{-1})$ result in dramatic improvement over previous studies with flash-lamp pumped dye lasers.

A laboratory computer controls the laser firing sequence and interfaces to detector analog and digital signals. In normal operation the experiments run from the computer under program control.

III. EXPERIMENTS

A. Time evolution of the ionization event

Any collisional ionizing process which depends on the population of real excited states will have a decay time characteristic of those states. By measuring the pulse shape of electron production we can determine if the ionizing process decays with excited-state population or extinguishes promptly with the laser pulse.

The experiment was performed in two ways: First, we used the CEM as shown in Fig. 1. Second, the particle multiplier, normally used for positive ion detection, was modified to measure negative charge. With the dye laser tuned to arbitrary positions away from any known atomic or molecular transition, the electron charge pulse produced by laser ionization was detected and displayed on a fast oscilloscope. The result from both experiments agreed. We observed a narrow, near-Gaussian-shaped pulse of about 20 nsec width in synchronism with the laser pulse. This result is direct confirmation that the ionizing mechanism varies promptly with the pulsed light field. The added 10 nsec of width is due to time dispersion in the time-of-flight collection and electronic detection systems. To check this result we tuned the dye laser onto a $Na(3s) \rightarrow Na^*(3p)$ transition to observe the time evolution of a known, conventional associative ionization collision,

$$Na^*(3p) + Na^*(3p) \rightarrow Na_2^+ + e \ . \tag{1}$$

As the laser was scanned through the atomic resonance, we observed a dramatic change in the electron time dependence. The pulse shape expanded to a width of about 150 nsec with a sharp (20-nsec) spike remaining on the leading edge. We attribute the sharp spike to two-photon ionization out of $Na^*(3p)$—a "prompt" effect. The wide plateau following the spike is due to process (1). Although the lifetime of isolated $Na^*(3p)$ against spontaneous emission is 16 nsec, radiation trapping significantly increases the apparent lifetime even at atomic densities as low as 10^{10} cm^{-3}. A recent paper by Garver et al.[16] underscores the importance of radiation trapping in alkali-metal resonance transitions. The experimental results prove that Na_2^+ is not produced by class 1c (optical pumping of X-state Na_2) nor by class-2 processes as discussed in Sec. I.

B. The Na_2^+ spectrum

Figure 2 shows the highly structured spectrum of Na_2^+ observed at a power density of about 1 MW/cm^2 and a spectral resolution of about 0.1 Å. The spectrum is precisely calibrated by four internal

Na_2^+ LASER SPECTRUM
and
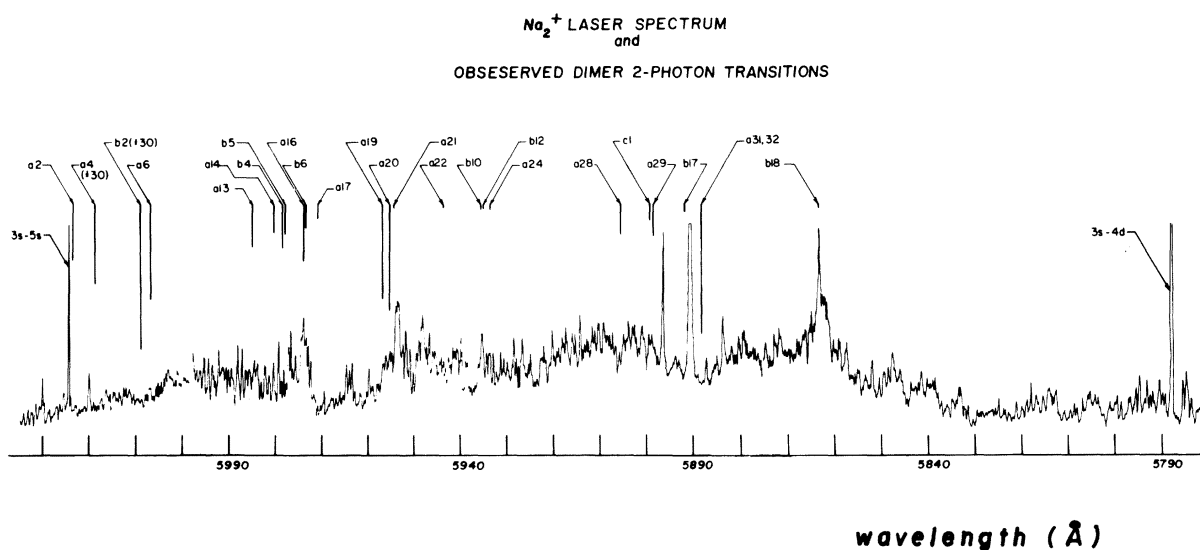OBSESERVED DIMER 2-PHOTON TRANSITIONS

wavelength (Å)

FIG. 2. Spectrum of Na_2^+ generated by intense, nonresonant optical radiation. Labeled lines are two-photon dimer transitions assigned by Doppler-free spectroscopy. Two intense peaks near 5890 Å are the resonance transitions $^2S_{1/2} \rightarrow ^2P_{1/2}$ and $^2S_{1/2} \rightarrow ^2P_{3/2}$ in atomic sodium.

markers: resonance spikes at the $3s \to 5s$ and $3s \to 4d$ two-photon transition and at the two fine-structure levels, $^2P_{3/2}, ^2P_{1/2}$, of the one-photon $3s \to 3p$ transition. Every structural feature is reproducible, even the smallest. Superimposed on the spectrum are the recent results of Morgan et al.[9] which identify the observed and assigned two-photon transitions in Na_2. The two spectra are compared to determine if all or some part of the Na_2^+ structure might be explained by dimer two-photon absorption followed by photoionization. Figure 2 shows relative intensities of the two-photon absorption peaks, calculated from the well-known perturbation expression for the transition probability,

$$P \propto \left[\frac{E^2 \sum_i \mu_{li} \mu_{iu}}{4\hbar^2 \Delta\omega_i} \right]^2 , \quad (2)$$

where μ_{li}, μ_{iu} are the transition dipole matrix elements between lower, intermediate, and upper states. The sum is over all intermediate states that couple the lower and upper levels. Radiation field power density is proportional to E^2 and $\Delta\omega_i$ is the detuning of the laser frequency from exact resonance with an intermediate state.

In practice usually only one intermediate rovibronic state dominates for each line shown in Fig. 2. The calculated relative intensities also include the rotation-vibration equilibrium population distributions evaluated at the source temperature. Lines assigned to $X\,^1\Sigma_g^+ \to$ to $^1\Sigma_g^+$ $(3s + 5s)$ transitions are labeled an, where n is the sequential numbering in Morgan's listing.[9] Lines assigned to $X\,^1\Sigma_g^+ \to {}^1\Sigma_g^+$ $(3s + 4d)$ are similarly labeled bn, and $X\,^1\Sigma_g^+ \to {}^1\Pi_g$ $(3s + 4d)$ transitions are labeled cn. Several salient points are worth noting. First, the absolute position of the dimer two-photon transitions are precise to well within 0.01 cm^{-1}, while the position of structural features in our Na_2^+ spectrum is limited by bandwidth (~ 0.1 cm^{-1}) in the dye-laser output. Therefore, to identify an Na_2^+ peak with a dimer two-photon transition, the two must coincide to within 0.1 cm^{-1}. A careful comparison reveals that only $b18$ meets this test, although $a16$ and $b6$ come close. Second, the number of two-photon dimer transitions is small compared to the dense packing of peaks in the Na_2^+ spectrum. As discussed by Morgan et al.[9] the relative rarity of intense two-photon molecular transitions in Na_2 is due to the infrequent occurrence of near-resonant intermediate-state couplings to the laser field [small $\Delta\omega_i$ in Eq. (2)]. This effect in turn is due essentially to dissimilar rotational constants in the X and A states. Thus a somewhat widely spaced, intense set of peaks should characterize two-photon alkali-metal dimer

spectra. It is evident that the Na_2^+ laser spectrum of Fig. 2 shows quite the opposite features—closely spaced structure with only small intensity variations. Third, no similar pattern of intensities can be discerned between the two spectra. Note that the most intense two-photon dimer transition $(b2)$ has no prominent Na_2^+ peak anywhere near it. Conversely although the strongest laser-induced Na_2^+ peak is coincident with $b18$, this two-photon transition has one of the smallest intermediate-state couplings.

Despite the lack of concordant peak positions, spectral density, and intensity, it is still not inconceivable that some of our observed structure is nevertheless due to dimers. The region around 6010 Å, for example, resembles a band head. Although the two-photon peaks do not match to within the required precision, a concentration of seven transitions in this region suggests a possible connection. Thanks to recent advances in high-resolution molecular spectrosocpy the Dunham coefficients for the relevant lower, intermediate, and upper states are now determined[9,11]; and a careful calculation of two-photon transition rates in this region, including all Franck-Condon factors, has become possible. We are presently carrying out calculations to locate expected strong dimer transitions possibly missed by Morgan's survey. We will report on this effort in the near future. It is clear from the present experimental evidence, however, that neither the position nor the intensity of the two-photon dimer transitions matches well the Na_2^+ spectrum observed in our experiments.

C. Laser-induced quenching of Na_2^+

Next we performed two double-laser experiments to investigate the sensitivity of Na_2^+ formation to the ground-state population of atomic sodium. Two light pulses, each from independent laser sources entered the collision region. The time delay between pulses could be varied continuously from 0 to 1500 nsec with a time jitter less than 1 nsec. The relatively low-intensity pulse ($\sim 10^4$ W/cm^2) from laser 1, a flash-lamp-pumped tunable dye laser, was trimmed to 300 nsec by a Pockels cell optical shutter which also defined the rising and falling edges of the light pulse to less than 1 nsec. Pulses from laser 2 were of 10-nsec duration and synchronization between lasers was adjusted so that laser pulse 2 entered the interaction-region 150 nsec after laser pulse 1. Laser 2 was the source of the same high-power pulses used to generate the spectrum in Fig. 2. With laser 1 tuned out of the Na resonance transition, no measurable effect was observed on the Na_2^+ spectrum produced nonresonantly by laser 2. Tuning laser 1 onto either fine-structure level of the $Na(3s) \to 3p$ transi-

Na$_2^+$ QUENCHING by
RESONANT 3-PHOTON
IONIZATION
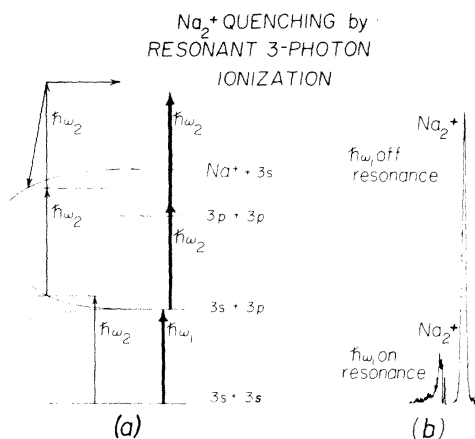

(a)   (b)

FIG. 3. Far left side (a) shows possible ionization pathway induced by nonresonant laser field. Right side (b) shows quenching effect of ground atomic state depopulation on Na_2^+ signal. Heavy arrows show how resonant population of $Na^*(3p)$ followed by two-photon ionization, preempts the laser-induced Na_2^+ formation thereby "quenching" dimer ion intensity.

tion, however, sharply "quenched" the Na_2^+ signal as illustrated on the right-hand side of Fig. 3. A dramatic enhancement of Na^+ intensity was observed at the same time.

The left-hand side of Fig. 3 shows two routes to ionization consistent with the observations: On the far left, laser 1 ($\hbar\omega_1$) is nonresonant and plays no role in the collision dynamics. Laser 2 is also nonresonant but with much higher power ($\sim 10^6$ W/cm^2) and produces the laser-induced ion signal. As laser 1 is tuned onto resonance the direct route to Na^+, via atomic two-photon ionization from the $3p$ level (denoted in Fig. 3 by heavy arrows), becomes the dominant process. A simple calculation of the upper limit to the laser-induced collisional ionization rate compared to resonance-enhanced three-photon ionization confirms that the latter rate[17] dominates. With laser 1 populating the resonance level laser 2 literally burns a hole in the atomic population, converting it to Na^+,

$$Na(3s) + \hbar\omega_1 \rightarrow Na^*(3p) ,$$

$$Na^*(3p) + 2\hbar\omega_2 \rightarrow Na^+ + e , \qquad (3)$$
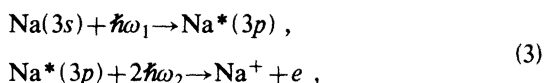
for lasers 1 and 2, respectively.

The marked quenching of Na_2^+ intensity simultaneous with hole burning in the atomic ground-state population is direct evidence for an *atomic* origin of Na_2^+ formation.

As a consistency check we performed a time-delay double laser experiment. Tuning of laser 1 was fixed at the atomic resonance transition; but the time de-

lay between it and laser 2 was systematically increased. The results in Fig. 4 show that rate of nonresonant Na_2^+ formation from laser 2 recovers after several hundred nanoseconds delay between it and the cutoff of laser 1. This observation is in agreement with the apparent lifetime of $Na^*(3p)$ due to radiation trapping and confirms that Na_2^+ derives from a ground-state population of Na.

D. Na_2^+ intensity versus Na and Na_2 density

By frequency doubling the dye-laser output and mixing it with the Nd^{3+}:YAG fundamental we produced a beam of uv photons around 2300 Å for the purpose of directly photoionizing Na and Na_2. From the known photoionization cross sections[18] and the measured relative intensities of the photoionized species the fractional abundance of Na_2 in the sodium beam was determined as a function of beam flux. Figure 5 shows that the dimer composition (open triangles) increases approximately as the square of atomic beam intensity. The uv and visible photon beams enter the collision region by opposite ports so that it is possible to alternately measure visible and uv generated ionization under exactly the same experimental conditions. It is clear from Fig. 5 that although the dimer concentration increases as the square of the atom concentration, Na_2^+ and Na^+ produced by intense visible light increase only linearly. If multiphoton photoionization of neutral dimers is responsible for dimer ions observed in the visible, then the intensity of Na_2^+ should linearly track the intensity of Na_2. Figure 5 shows that it does not. The results of this experiment therefore reinforce the conclusion of Sec. IV C, that Na_2^+ and Na^+ produced in the visible do not have a neutral dimer origin.

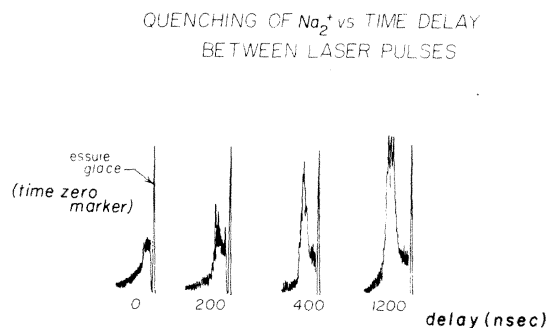QUENCHING OF Na$_2^+$ vs TIME DELAY
BETWEEN LASER PULSES

FIG. 4. Increasing time delay between resonant ($\hbar\omega_1$) and nonresonant ($\hbar\omega_2$) laser pulses shows that Na_2^+ intensity increases as atomic ground state is repopulated. Apparent excited-state lifetime lengthened by radiation trapping.
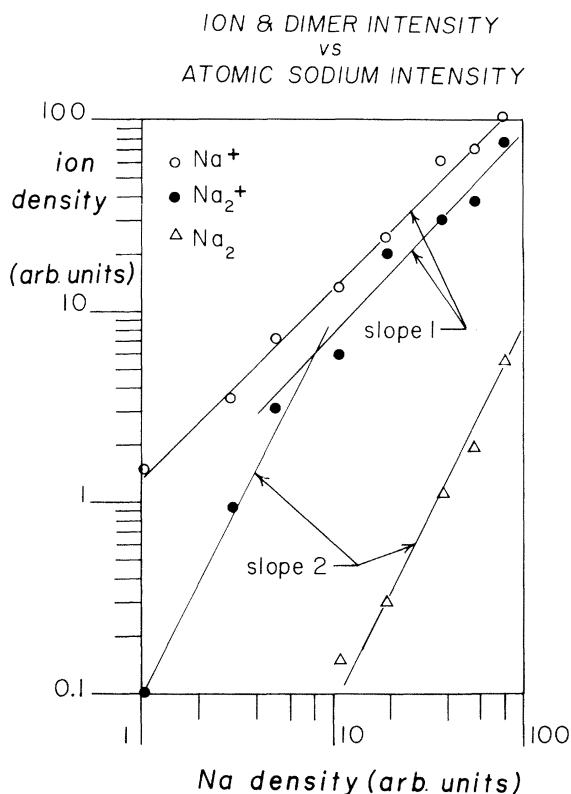
ION & DIMER INTENSITY
vs
ATOMIC SODIUM INTENSITY

FIG. 5. Na_2 density vs Na density measured directly by uv photoionization at 2300 Å. The Na^+ and Na_2^+ signals are produced by intense visible laser in the same experiment. Note that at low atom density Na_2^+ appears to increase quadratically but then becomes nearly linear as Na concentration increases. Note that Na^+ and Na_2^+ intensities are not linear functions of dimer density.

The slopes of the log-log plots in Fig. 5 do not lend themselves to simple interpretation. Two results require explanation: (1) the quadratic dependence of the neutral Na_2 dimer and (2) the nearly linear behavior of the laser-induced ionization (both as a function of Na atomic beam intensity).

One might suppose that the quadratic dependence of Na_2 on Na results from the law of mass action in thermodynamic equilibrium,

$$[Na_2] = K_{equil}[Na]^2 .$$ (4)

In practice, however, sodium beam intensity is increased by raising the primary oven temperature over the range from 200 to 350 °C. The equilibrium constant itself is a strongly decreasing function of temperature in the same range. Thus the temperature dependence of K_{equil} and [Na] tend to offset each other. A straightforward calculation of K_{equil} versus temperature from the rovibrational partition function of Na_2 agrees with experiment[19] and shows

that a log-log plot of dimer concentration versus atom concentration should exhibit a slope less than 1.5. It would be possible to rationalize the observed quadratic dependence by assuming that equilibrium is controlled by the secondary (nozzle) oven whose temperature is held constant throughout the experiment. However, a study of dimer intensity versus nozzle temperature (Sec. III E below) shows that vapor thermal equilibrium within the nozzle is never achieved.

Furthermore, the near-linear dependence of laser-induced Na^+ and Na_2^+ with atomic sodium density cannot be explained by elementary considerations. The obvious expectation is a quadratic dependence on Na density since the collision is bimolecular,

$$Na + Na + 3\hbar\omega \rightarrow Na_2^+ + e .$$ (5)
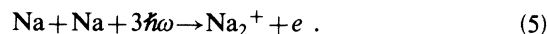
Possibly the collision dynamic involves the formation of a loosely bound intermediate whose lifetime against dissociation may decrease strongly with temperature and thus tend to offset the effect of increased atom density. This conjecture will be discussed more fully in Sec. IV.

E. Na^+ and Na_2^+ intensity versus nozzle temperature

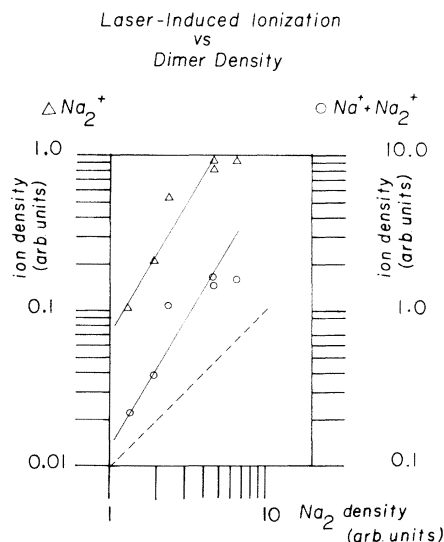In the final study of this series the conditions of the previous experiment were reversed. Tempera-

Laser-Induced Ionization
vs
Dimer Density

FIG. 6. Na_2^+ and $(Na^+ + Na_2^+)$ vs Na_2 density. Note that the left-hand ordinate denotes Na_2^+ and the right-hand ordinate denotes total ion yield $(Na^+ + Na_2^+)$. Dimer density, Na^+, and Na_2^+ intensity varied by increasing source nozzle temperature. Dashed line indicates expected slope if neutral dimers were source of laser-induced ionization.

ture in the primary oven was held constant while the secondary oven was heated in stages to a temperature of about 800 °C. Direct uv photoionization of the dimer was recorded alternately with Na$^+$ and Na$_2^+$ produced by visible light. Signals arising from both uv and visible light showed a marked decrease with increasing temperature. However, Fig. 6 shows that the visible signals fall more rapidly with temperature than the dimer population. The decrease in dimer concentration with nozzle temperature is due to partial thermal dissociation. Applying Eq. (4) together with the temperature dependence of K_{equil}, one quickly sees however that thermal dissociation of Na$_2$ in the nozzle is incomplete. The observed fractional dimer abundance as a function of temperature is always greater than that predicted by equilibrium. The results show that laser-induced ions vary more sensitively with temperature than does dimer thermal dissociation. Once again this finding is inconsistent with the dimer hypothesis that Na$_2^+$ observed in the visible results from multiphoton photoionization of Na$_2$ dimer.

IV. DISCUSSION

From the foregoing we conclude that of all the processes listed in Sec. I, those in category 3, laser-induced atomic collisions, are in best accord with experimental observation. If present, long-range interactions will dominate the collision dynamics, and in this case *resonant* dipole-dipole forces between the approaching partners produce splitting of molecular states which derive from the Na(3s)+Na*(3p) levels. The states separate as the inverse cube of the internuclear distance. The situation is analogous to that for Li + Li optical collisions discussed previously[12] in which the asymptotic levels split symmetrically into four states, $\Pi_{u,g}$ and $\Sigma_{u,g}$, in the singlet and triplet spin manifolds, respectively. Figure 7 shows how these very-long-range quasimolecule states may be populated by off-resonant radiation. In simplest terms the process may be regarded as a localized photon adsorption around the region of radial separation where the energy difference between molecular states is in resonance the photon energy. After transition onto one of the excited states two routes are possible: (1) a prompt ionizing two-photon absorption mediated through higher-lying molecular levels (top panel of Fig. 7) or (2) the formation of a long-lived quasimolecule defined by a shape or Feschbach resonance, with subsequent photon absorption to the electron continuum (bottom panel of Fig. 7). In route (1) the ionizing photon absorption is coherent with the initial optical collision and takes place at far internuclear separation. In route (2) a well-defined collision resonance is pro-
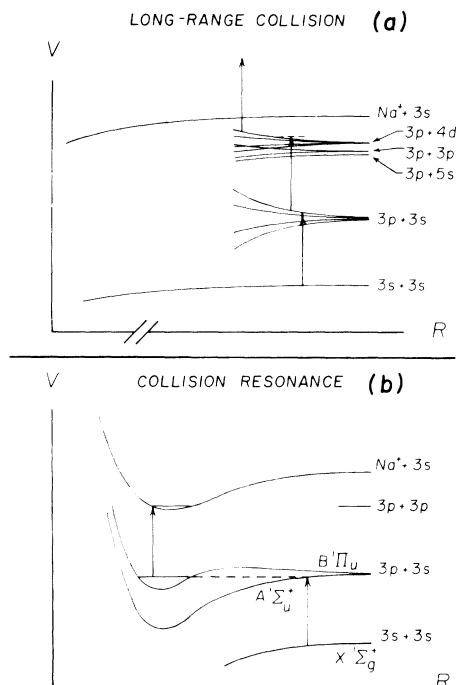

FIG. 7. Upper panel (a) shows a suggested mechanism in which multiphoton absorption occurs through quasi-molecular potential curves formed by long-range collisional interaction. Bottom panel (b) shows a contrasting collision dynamic in which a long-lived collision complex is first formed by photon absorption at long range followed by photoionization of the complex at short range. The actual pathway shown is only one of several possibilities.

duced at shorter range. Only after collision partners are trapped behind a barrier (either centrifugal or potential) does photoionization of the collision complex take place. Thus the photoionization step need not be simultaneous with the initial optical collision.

Following the perturbation development outlined earlier[12] we find that the probability P for populating an excited molecular state at long range is given by,

$$P = \frac{\pi E^2}{\hbar^4} \left[\frac{2}{3\hbar} \frac{1}{4\pi\epsilon_0} \right]^{1/3} \left[\frac{\mu_{12}^2}{\Delta\omega} \right]^{4/3}, \qquad (6)$$

where μ_{12} is the transition dipole moment between lower and upper molecular states, $\Delta\omega = \omega - \omega_0$ is the detuning of laser frequency ω from the *atomic* transition frequency ω_0, and E^2 is proportional to the laser field intensity. Taking $\mu_{12} = 5.2 \times 10^{-29}$ C m and $\Delta\omega = 100$ cm^{-1}, expression (6) yields a probability of about 0.26 with a laser power density of 1 MW/cm^2. Thus we see that even at moderate field

intensity laser-induced population of the molecular excited-state manifold is quite significant. In fact above 1 MW/cm^2 the perturbation assumption rapidly breaks down as the time of passage through the "crossing point" in Fig. 7 becomes comparable to the Rabi period.

After the system transfers to the initial excited curve via the optical collision route, the top panel of Fig. 7 shows how it may rapidly absorb two more photons while the partners are still at very far internuclear separation. The rate for this second, two-photon step depends strongly on the relative position of the higher-lying excited states which mediate the absorption. It is hoped that ab initio and model potential calculations[20] of the relevant curves (correlating to atomic levels $3p + 5s$, $3p + 3p$, and $3p + 4d$) will help decide the importance of this route to Na_2^+.

An alternate pathway to ionization is through collision resonances, the laser-assisted dynamics of which have recently been considered by Hutchinson and George.[21] In the present case, rather than immediate two-photon absorption after the optical collision step, the two atoms continue to approach until they encounter a barrier. If the relative kinetic energy is slightly less than the barrier height, tunneling through the barrier may trap the collision partners in a shape resonance. A variation on this theme is inverse predissociation in which the partners approach on one molecular curve without a barrier and undergo a free-bound electronic transition inside the barrier of a second potential curve. Yet another variation is an optical collision to a bound state without a barrier followed by a bound-bound "internal conversion" to a second electronic state with a barrier. This latter route is specifically illustrated in the bottom panel of Fig. 7. Both shape resonances[22] and Feschbach resonances[23] have been considered as collision intermediates to radiative association,

$$A + B \rightarrow [AB], \text{ with } k_1 \text{ (resonance formation)}, \quad (7a)$$
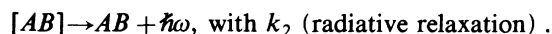
$$[AB] \rightarrow AB + \hbar\omega, \text{ with } k_2 \text{ (radiative relaxation)}. \quad (7b)$$

These earlier studies were motivated by interstellar molecular formation in environments where the only important radiative process was spontaneous emission. The same analysis, however, may be applied to the present case where stimulated photon absorption

out of the collision resonance will be the dominant "relaxation" mechanism. In analogous fashion the overall rate constant for the associative ionization process may be written in terms of the two constituent steps,

$$Na + Na \rightarrow [Na_2], \quad (8a)$$
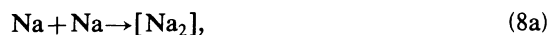
with Γ_c (resonance formation),

$$[Na_2] + n\hbar\omega \rightarrow Na_2^+ + e, \quad (8b)$$
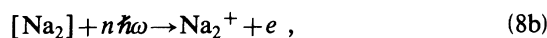
with Γ_p (photoionization).

The overall rate constant is written,

$$k_i = \hbar^2 \left[\frac{2\pi}{\mu kT} \right]^{3/2} (2J_i + 1) \left[\frac{\Gamma_c \Gamma_p}{\Gamma_c + \Gamma_p} \right] e^{-E_i/kT}, \quad (9)$$

where E_i is the energy and J_i angular momentum quantum number associated with resonance level i, μ is the reduced mass of the two-body collision, and Γ_c, Γ_p are the collision and photoionization "widths," respectively. These widths are related to the lifetime against dissociation and photon absorption by $\Gamma_c = \tau_c/\hbar$ and $\Gamma_p = \tau_p/\hbar$. In order to apply Eq. (9) the potential-energy curves must be accurately known, to within about 10 cm^{-1}. Furthermore, calculation of Γ_c and Γ_p requires free-bound or bound-bound coupling matrix elements themselves obtainable only from highly reliable bound and free vibrational wave functions. Although calculations of the relevant Rydberg-Klein-Rees potential curves and collisional couplings are more tractable for Na_2 and Li_2 than for other small-molecule systems, we are not yet able to apply in detail Eq. (9) to the spectrum of Fig. 2. Efforts in this direction are continuing, but a present one can only observe that the densely packed structure of the Na_2^+ spectrum together with the strong sensitivity to temperature suggests the predominance of a bound collisional intermediate over a purely long-range mechanism.

ACKNOWLEDGMENTS

---

*Permanent address: Institut de l'Electronique Fondamentale, Université de Paris—Sud, Bâtiment 220, F-91405 Orsay, France.

[1]P. Polak-Dingels, J.-F. Delpech, and J. Weiner, Phys.

Rev. Lett. 44, 1663 (1980).
[2]F. Roussel, B. Carré, P. Berger, and G. Spiess, J. Phys. B 14, L313 (1981).
[3]A. v. Hellfeld, J. Caddick, and J. Weiner, Phys. Rev.

Lett. <u>40</u>, 1369 (1978).

[4]J. Weiner, J. Chem. Phys. <u>72</u>, 2856 (1980).

[5]P. Polak-Dingels and J. Weiner, J. Chem. Phys. <u>74</u>, 508 (1980).

[6]P. Polak-Dingels, J.-C. Gauthier, J. Keller, M. Bras, and J. Weiner, Phys. Rev. A <u>24</u>, 1107 (1981).

[7]J. P. Woerdman, Chem. Phys. Lett. <u>43</u>, 279 (1976).

[8]H.-R. Xia, G.-Y. Yan, and A. L. Schawlow, Opt. Commun. <u>39</u>, 153 (1981).

[9]G. P. Morgan, H.-R. Xia, and A. L. Schawlow, J. Opt. Soc. Am. <u>72</u>, 315 (1982).

[10]C. Y. R. Wu (private communication).

[11]N. W. Carlson, A. J. Taylor, K. M. Jones, and A. L. Schawlow, Phys. Rev. A <u>24</u>, 822 (1981).

[12]P. Polak-Dingels, R. Bonanno, J. Keller, J.-C. Gauthier and J. Weiner, Phys. Rev. A <u>25</u>, 2539 (1982).

[13]T. B. Lucatorto and T. J. McIlrath, Appl. Opt. <u>19</u>, 3948 (1980), and references cited therein.

[14]P. Polak-Dingels, J. Keller, R. Bonanno, and J. Weiner, J. Phys. B <u>15</u>, L41 (1982).

[15]A detailed description of this technique will be published shortly in a study of Rydberg-state associative ionization.

[16]W. P. Garver, M. R. Pierce, and J. J. Leventhal, J. Chem. Phys. <u>77</u>, 1201 (1982).

[17]C. Laughlin, J. Phys. B <u>11</u>, 1399 (1978).

[18]R. D. Hudson, Phys. Rev. <u>135</u>, A1212 (1964).

[19]C. T. Ewing, J. P. Stone, J. R. Spann, and R. R. Miller, J. Phys. Chem. <u>71</u>, 473 (1967).

[20]Professor D. Konowalow of State University of New York, Binghamton and Professor F. Masnou of the University of Paris both report progress in the calculation of some of these curves (private communication).

[21]M. Hutchinson and T. F. George, Phys. Lett. <u>82A</u>, 119 (1981).

[22]R. A. Bain and J. N. Bardsley, J. Phys. B <u>5</u>, 277 (1972).

[23]P. S. Julienne and M. Krauss, in *Molecules in the Galactic Environment*, edited by M. A. Gordon and L. E. Snyder (Wiley, New York, 1973).